# Electrochemical Investigation of Localized CO$_2$ Corrosion on Mild Steel

Jiabin Han, Yang Yang, Bruce Brown, Srdjan Nesic
Institute for Corrosion and Multiphase Technology,
Department of Chemical and Biomolecular Engineering
Ohio University
342 West State Street,
Athens, Ohio 45701

## ABSTRACT

Localized CO$_2$ corrosion on mild steel is always associated with the partial breakdown of a protective corrosion product scale such as iron carbonate. The scale breakdown can happen for a variety of reasons many of them related to fluid flow. It is hypothesized that following the scale damage, a galvanic effect is established between the scale covered surface (cathode) and the scale free surface (anode) leading to propagation of localized attack.

To test this hypothesis, in a series of laboratory experiments, an iron carbonate scale is formed by a repeatable process. Subsequently, in the so called "scale removal tests" the breakdown of the scale under flowing conditions is investigated. The results show that the iron carbonate scale can be partially removed by mechanical stresses, chemical dissolution or by both mechanisms acting simultaneously. In another series of experiments, a newly developed "artificial pit" test is used to investigate the propagation of localized CO$_2$ corrosion via a galvanic coupling. The artificial pit is composed of a large cathode covered by protective iron carbonate scale, and a small bare steel anode. The two are electrically isolated and connected by a zero resistance ammeter to measure the galvanic current during the tests. The results have confirmed the galvanic mechanism for localized CO$_2$ corrosion propagation. It has been demonstrated that pits will propagate only if the conditions are just right: the solution is neither undersaturated nor heavily supersaturated with respect to iron carbonate, i.e. they are in the so called "grey zone".

# INTRODUCTION

Hazardous failures to mild steel pipelines in the oil and gas industry are most frequently caused by localized corrosion. Localized attack penetrates the pipeline wall in a rather short period of time and is difficult to predict or detect. This issue is attracting attention from the industry and academia alike, [1-17] but the topic still remains open for further investigation, as some of the key questions remain unanswered.

It is believed that at least two main steps are involved in the localized corrosion process: *initiation*, and *propagation*. In $CO_2$ environments, a protective iron carbonate ($FeCO_3$) scale may form on the steel surface as a by-product of the corrosion process. Any localized damage to this scale may be one of the ways to initiate localized corrosion. Some initial work has been done in rotating-cylinder glass-cell experiments on scale removal mechanisms which were found to be associated with hydrodynamic forces and chemical dissolution [18]. Compared to that work, a more realistic scale formation method is used in the current study. The mechanism of localized attack propagation was studied here in a newly developed experimental setup inspired by Turnbull's "pencil pit" [19, 20]. The original design has been improved and modified to make it more versatile and realistic and is referred to below as the "artificial pit" (AP). It is well known that in some cases localized corrosion is initiated but it does not propagate. It has been suggested that for propagation to happen the water chemistry has to be neither undersaturated nor supersaturated with respect to iron carbonate. In the former case this leads to scale dissolution and overall general corrosion at a very high rate. In the latter case, when the water is supersaturated, low uniform corrosion rates prevail due to the "healing" of scale damage by scale re-growth. When the conditions are in between, i.e. in the "grey zone" [17] localized propagation is expected. Using the AP test, this concept is investigated and reported below.

# EXPERIMENTAL

## Experimental setup

Two different experimental setups were used for testing: localized corrosion *initiation* by scale removal and localized corrosion *propagation* due to galvanic effect, as described below.

### Test setup: scale removal (for investigation of localized corrosion initiation)

The glass cell set-up used in the scale removal experiment is shown in Figure 1, in which the rotating cylinder electrode is used as the working electrode (WE). An additional identical cylindrical coupon has been added to the glass cell at the beginning of the experiment which is removed after the scale formation process, and is used to visually inspect the specimen prior to scale removal and confirm the repeatability of the scale formation process. A concentric stainless steel ring served as a counter electrode (CE) and a saturated silver/silver-chloride (Ag/AgCl) electrode (SSE) served as a reference electrode (RE). The test matrix for scale formation and scale removal is shown in Table 1.

In mechanical scale removal, prior to rotation at high speed (up to 7000 rpm, wall-shear stress 45 Pa), the solution was adjusted to be just above the saturation level, in order to prevent further precipitation as well as any scale dissolution. In chemical scale removal, the solution was adjusted to be below the saturation point and very low rotation speed (100 rpm, wall-shear stress 0.03 Pa) was used in order to

minimize mechanical scale damage. For a combined chemo-mechanical scale removal, an under saturated solution and a higher rotating speed were used simultaneously.

<u>Test setup: artificial pit (for investigation of localized corrosion propagation)</u>

A new test design was employed that accurately mimics the behavior of a single pit. It is known that localized $CO_2$ corrosion frequently appears in the form of mesa attack i.e. a scale covered protected steel surface surrounds a flat bare metal section of the steel wall which is corroding at a very high rate (see sketch in Figure 2). The inspiration for the new test design that would capture this behavior was taken from Marsh, et al [19] and Turnbull [20] who investigated the effect of inhibitors on localized corrosion. In their design the anode and cathode were isolated from each other in order to measure any galvanic coupling resulting in localized corrosion. However, the two electrodes were also physically separated, in Marsh's case within a single cell while in Turnbull's case between two glass cells connected with a salt bridge. The latter made it easier to control the separate environments but has also introduced problems. In both cases, the most serious drawback is related to the physical separation of the anode and cathode which gives rise to Ohmic resistance, particularly so in the aqueous phase, during any galvanic current measurements. In reality the anode and the cathode are part of the same steel surface in very close proximity and this was accounted for in the new artificial pit design.

The overall AP glass cell test setup is shown in Figure 3. In a classical three electrode electrochemical arrangement as described above, the AP replaces the working electrode. The detailed view of the AP is given in Figure 4. The cathode is a (16 $cm^2$) cylindrical steel surface much larger than the small cylindrical anode (0.018 $cm^2$) which is inserted through the center of the cathode and is electrically isolated from it. The surface area ratio between cathode and anode is almost 900 which is similar to previous designs [19, 20]. The surface of the anode can be mounted flush or receded with respect to the cathode surface. The two are connected by a zero resistance ammeter (ZRA) during galvanic current measurements and disconnected during potential and polarization resistance measurements.

**Experimental procedure**

<u>Test procedure: scale removal (for investigation of localized corrosion initiation)</u>

1. Prepare a 1wt% NaCl solution, deaerate the solution with $CO_2$, and heat to 80$^o$C.
2. Adjust the pH to 6.3 by adding a deaerated $NaHCO_3$ solution.
3. Add 200 ppm $FeCl_2$ to achieve a high concentration of $Fe^{2+}$ and the desired supersaturation of iron carbonate.
4. Prepare coupons by polishing with 200, 400 and 600 grit sand papers in succession; during polishing keep rinsing the coupons with alcohol to prevent the surface from overheating, to dehydrate it and to remove the iron particles left on the surface.
5. Put the coupons into an alcohol bath and clean them by using an ultrasonic cleaner and dry.
6. Insert them into the prepared solution and use the LPR method to measure the corrosion rate as the iron carbonate scale develops.
7. When the corrosion rate becomes stable and less than 0.1mm/yr, the scale formation process is finished.
8. Remove one coupon, rinse with alcohol immediately, dry, store in the desiccator for SEM characterization of the initial scale surface.
9. Adjust the pH slightly by adding a deaerated $NaHCO_3$ or a dilute HCl solution according to the water chemistry calculations to achieve the conditions for mechanical and/or chemical scale removal.

10. Adjust the rotating speed (7000 rpm and 1000rpm for mechanical removal and 100 rpm for chemical removal).
11. Measure the corrosion rate by LPR method during the scale removal process.
12. When the experiment stops, remove the second coupon and rinse with alcohol immediately, dry, store in the desiccator for SEM characterization of the scale surface after mechanical and/or chemical attack.

Test procedure: artificial pit (for investigation of localized corrosion propagation)

1. Prepare the aqueous solution according to steps 1 – 3 listed above.
2. Before exposure to the corrosive environment, the two steel surfaces, cathode and anode, are prepared in the same way as described in points 3 and 4 above.
3. Cathode is inserted into the prepared solution and the LPR method is used to measure the corrosion rate as the iron carbonate scale develops.
4. When the corrosion rate becomes stable and less than 0.1mm/yr, the scale formation process on the cathode is finished.
5. The solution pH is adjusted to the desired value by adding a deaerated $NaHCO_3$ or a dilute HCl solution according to the water chemistry calculations.
6. The small anode is inserted through a compression fitting to a predetermined depth with respect to the cathode surface.
7. Galvanic current between anode and cathode is recorded using ZRA (Zero Resistance Amperemeter). The anode and cathode are disconnected occasionally for a very short time (< 1 minute) to record open circuit potentials and corrosion current by LPR.


## RESULTS AND DISCUSSION

As many conflicting statements can be found in the open literature on the subjects presented below, accompanied by very little explicit proof, the following discussion will be presented in the form of a series of hypotheses derived from the literature, which are then tested by the results obtained in this study.

**Initiation of localized corrosion - scale removal experiments**

In all the cases, iron carbonate scales were formed under nominally identical condition, as shown in the test matrix. The change of the corrosion rate during the scale formation process is shown in Figure 5. While there was considerable variation in the appearance of the curves (which was difficult to avoid), after approximately 50 to 60 hours, the corrosion rate decreased to less than 0.1mm/yr in all the experiments, which proved that a protective scale was formed on the surface of the coupon. Due to the precipitation of $FeCO_3$ from the solution, the pH was spontaneously reduced from the initial pH6.3 to approximately pH6.1 by the end of scale formation period as $Fe^{2+}$ ions were consumed during precipitation.

Hypothesis #1. Mechanical scale removal:

"*Iron carbonate scales cannot be removed by hydrodynamic forces alone, their mechanical strength is too high and mechanical forces induced by the flow are too low to cause any scale damage.*"

The change of corrosion rate during scale removal process under pH6.1, 1000rpm (wall-shear stress 2 Pa) and 7000rpm (wall-shear stress 45 Pa) rotating speed are shown in Figure 6 and Figure 8 respectively. Clearly there appears to have been scale removal in both cases with the higher rotation speed leading to a higher scale removal rate as indicted by a faster increase (higher slope) of the corrosion rate curve. The corresponding SEM pictures which are shown in Figure 7 and Figure 9, confirm these findings. It can be seen that there is much less iron carbonate scale remaining on the surface of the steel after exposure to flow in both cases, confirming that the increase of the corrosion rate in Figure 6 and Figure 8 is due to the partial removal of the protective scale. One can also notice in Figure 9 what appears to be an initiation of localized attack at the higher flow rate. Clearly Hypothesis #1 needs to be rejected, and conclude that iron carbonate scales are prone to mechanical scale removal even at very low flow rates.

Hypothesis #2. Chemical scale removal:

"*Iron carbonate scales can be rapidly dissolved away by slightly under-saturated solutions*"

After the iron carbonate scale was exposed to an under-saturated solution, dissolution started immediately as indicated by the corrosion rate curves obtained for pH5.8 and pH 5.6 which are shown in Figure 10 and Figure 12 respectively. Higher scale removal rate is seen at the lower pH as expected. Figure 11 and Figure 13 show the SEM pictures of the steel surface before and after scale removal experiments. It clearly can be seen that most of the smaller crystals were removed by dissolution, which is responsible for the increase of the corrosion rate. The edges of the crystals which remained on the surface in Figure 11 and Figure 13 are not as sharp as prior to the chemical attack, which is a signature of a chemical dissolution process. Undoubtedly, hypothesis #2 was confirmed.

Hypothesis #3. Combined chemo-mechanical scale removal

"*There exists a significant synergy between the mechanical and chemical modes of iron carbonate scale removal*"

Results from the combined chemo-mechanical removal of the iron carbonate scale are shown in Figure 14 for a low under-saturation and low velocity (pH5.8, 1000rpm) and Figure 16 for a high under-saturation and a high velocity (pH5.6, 7000rpm). Figure 15 and Figure 17 show the corresponding SEM images of the steel surface before and after the scale removal experiments. Very little original iron carbonate scale has survived and one can even observe initiation of localized corrosion of the underlying steel in both cases. It is speculated that the partial removal of the iron carbonate scale may lead to galvanic effect which will cause localized corrosion, and this is discussed in the following heading.

Figure 18 and Figure 19 show the summary of the scale removal rates as expressed by the slopes of the corrosion rate curves seen in previous plots. One can conclude that significant synergy was detected in both cases, i.e. Hypothesis #3 was confirmed.

**Propagation of localized corrosion – artificial pit tests**

Hypothesis #4

"*The potential of a mild steel surface covered with a protective iron carbonate scale is significantly higher than the potential of a bare steel surface exposed to the same conditions*"

To prove this point, Figure 20 shows the typical scale formation process on the cathode during the first stage of the AP test. It can be observed that the general corrosion rate is reduced to rather low values after a day of exposure. The open circuit (corrosion) potential first decreases somewhat and then increases during the scale removal process. The difference between the open circuit potentials of the iron carbonate covered surface at the end of the experiment and the bare metal surface at the beginning of the experiment is 20-30mV, under these conditions. Basic electrochemical theory, based on diffusion limiting or blockage effects actually suggests the opposite; however a detailed discussion of this issue exceeds the scope of the present paper and will be published separately. What is important to notice is that the scale covered surface does reach a higher potential and will act as a cathode when connected with a bare steel surface which would become the anode. In reality this can readily happen when the scale is locally removed by mechanical and/or chemical means as described in the section above. When the surface area of the scale covered cathode is much larger than the surface area of the bare metal anode, the anode is polarized anodically as shown in Figure 21. Notice that the coupled potential is determined by the larger surface area cathode. In summary, Hypothesis #4 has been confirmed.

Hypothesis #5

"*The potential difference between anode and cathode may lead to a significant galvanic current*"

As mentioned in the AP test procedure description above, the open circuit potentials of anode and cathode can be measured when they are disconnected, while the mixed potential (or coupled potential) and any resulting galvanic current (coupling current) can be measured when they are connected via a ZRA. Examples of data collected under different conditions are shown in Figure 21, Figure 22 and Figure 23. The black solid rectangles represent the magnitude of the *driving force* (the disconnected potential difference between anode and cathode), and the line shows the *resulting galvanic current density* as a function of time, when they are connected. It is obvious that when the driving force is large i.e. open circuit potential difference between anode and cathode is high then the galvanic current density is also high and vice versa. It should be noted that the current densities shown in Figure 22 and Figure 23 are calculated based on the anode surface area. Once can conclude that the explicit proof is presented for Hypothesis #5 what enables us to generalize that localized $CO_2$ corrosion can propagates when a stable difference in corrosion potential is established between a large-area mild steel surface covered by a protective iron carbonate scale and a small-area bare steel surface corresponding to bottom of a pit or a mesa.

Hypothesis #6

"*Localized $CO_2$ corrosion always propagates when there is a galvanic coupling between a large cathode covered by a protective iron carbonate scale and a small bare metal anode*."

To test this hypothesis, galvanic current densities at different iron carbonate supersaturation levels are shown in Figure 24 to Figure 27. Supersaturation (SS) is defined as the degree of departure from thermodynamic equilibrium:

$$ SS = \frac{[Fe^{2+}][CO_3^{2-}]}{K_{sp}} $$

where, $[Fe^{2+}]$ is the concentration of iron ion; $[CO_3^{2-}]$ is the concentration of the carbonate ion; $K_{sp}$ is the solubility product for $FeCO_3$ which is a function of temperature and ionic strength [21-28]. The results

indicate that very high galvanic currents (localized corrosion propagation rates) are obtained initially in all cases. However, when $FeCO_3$ supersaturation is high (Figure 24), the galvanic current density reduces to zero in two hours, indicating that initial localized corrosion did not propagate due to the scale formation on the anode, i.e. the "pit healed" as the corrosion potentials on both cathode and anode equalized and corrosion rates remained low (<0.1 mm/y). When $FeCO_3$ supersaturation is low (Figure 25), the galvanic current density also gradually reduces to zero, in this case because the protective scale on the cathode dissolves and the driving force for the galvanic coupling (potential difference) disappears. Both the anode and cathode experienced stable high uniform corrosion rates (>1 mm/y) in this case.

However, when iron carbonate supersaturation is in between i.e in the "grey zone" (SS=0.5-2)[*], the galvanic current remained at a high value throughout the experiment which means the localized corrosion propagated at a high rate. As shown in Figure 26, the galvanic current stabilized at a value which correspond to a localized corrosion rate of approximately 5 mm/y in contrast with the cathode which corroded at <0.1 mm/y at the same time. When the NaCl concentration increased to 10 wt% (Figure 27), the initial current is as high as 50 $A/m^2$ and then stabilizes at 19 $A/m^2$ which corresponds to catastrophically high localized corrosion rates (>20 mm/y). Similar results were obtained for receded pits (2mm) however the presentation of these results exceeds the scope of this paper.

These results clearly demonstrate that when the solution is "near saturation" with respect to iron carbonate i.e. in the "grey zone", favorable conditions are reached for localized corrosion propagation. In these conditions, the protective scale existing on the cathode will not dissolve while the anode will remained bare or covered with some non-protective scale, and the galvanic coupling will be sustained. In all other conditions, i.e. in highly super- or under-saturated solutions, localized corrosion will not propagate, i.e. Hypothesis #6 has to be rejected.

## CONCLUSIONS

1. Protective iron carbonate scales can be partially removed by hydrodynamic forces acting on the scale surface and by chemical dissolution of the scale, which may lead to initiation of localized corrosion.
2. Significant synergy exists between these two modes of protective scale removal.
3. The open circuit potential difference between a bare steel anode and an iron carbonate film covered cathode is the important driving force in localized $CO_2$ corrosion propagation process.
4. Localized $CO_2$ corrosion propagates only when the iron carbonate supersaturation is in the range of SS=0.5 - 2, i.e. the "grey zone" criterion.

## REFERENCES

1. Z. Xia, K.-C. Chou and Z. Szklarska-Smialowska, "Pitting Corrosion of Mild steel in $CO_2$-Containing NaCl Brine", Corrosion, Vol. 45, No. 8, 1989, pp. 636-642.
2. K. Videm and A. Dugstad, "Corrosion of Mild steel in an Aqueous Carbon Dioxide Environment. Part 1: Solution Effects", Material Performance, March, 1989, pp. 63-67.

---

[*] There is no sharp limit for the "grey zone" the numbers SS=0.5 and SS=2 should be taken only as indicative.

3. K. Videm and A. Dugstad, "Corrosion of Mild steel in an Aqueous Carbon Dioxide Environment. Part 2: Scale Formation", Material Performance, April, 1989, pp. 46-50.
4. R. Nyborg and A. Dugstad, "Mesa Corrosion Attack in Mild steel and 0.5% Chromium Steel", CORROSION/98, paper No. 29 (Houston, TX: NACE, 1998).
5. R. Nyborg, "Initiation and Growth of Mesa Corrosion Attack during $CO_2$ Corrosion of Mild steel", CORROSION/98, paper No. 48 (Houston, TX: NACE, 1998).
6. R. Nyborg and A. Dugstad, "Understanding and Prediction of Mesa Corrosion", CORROSION/2003, paper No. 642 (Houston, TX: NACE, 2003).
7. M. H. Achour, J.Kolts, A. H. Johannes and G. Liu, "Mechanistic Modeling of Pit Propagation in $CO_2$ Environment under High Turbulence Effects", CORROSION/93, paper No. 87, (Houston, TX: NACE, 1993).
8. G. Schmitt and M. Horstemeier, "Fundamental Aspects of $CO_2$ metal Loss Corrosion – Part II: Influence of Different Parameters on $CO_2$ Corrosion Mechanism", CORROSION/2006, paper No. 06112, (Houston, TX: NACE, 1993).
9. G. Schmitt, W. Bucken and R. Fanebust, "Modeling Microturbulences at Surface Imperfections as Related to Flow – Induced Localized Corrosion", Corrosion, Vol. 48, No. 5, 1991, pp. 431-440.
10. G. Schmitt, T. Gudde and E. Strobel-Effertz, "Fracture Mechanical Properties of $CO_2$ Corrosion Product Scales and Their Relation to Localized Corrosion", CORROSION/96, paper No. 9, (Houston, TX: NACE, 1996).
11. G. Schmitt, C. Bosch, U. Pankoke, W. Bruckhoff and G. Siegmund, "Evaluation of Critical Flow Intensities for FILC in Sour Gas Production", CORROSION/98, paper No. 46, (Houston, TX: NACE, 1998).
12. G. Schmitt, M. Mueller, M. Papenfuss and E. Sttrobel-Effertz, "Understanding Localized $CO_2$ Corrosion of Mild steel from Physical Properties of Iron Carbonate Scales", NACE CORROSION/99, paper No. 38 (Houston, TX: NACE, 1999).
13. G. Schmitt, M Mueller, "Critical Wall Shear Stresses in $CO_2$ Corrosion of Mild steel", CORROSION/2002, paper No. 44, (Houston, TX: NACE, 1999).
14. G. Schmitt, C. Bosch, P. Plagemann and K. Moeller, "Local Wall Shear Stress Gradients in the Slug Flow Regime – Effect of Hydrocarbon and Carrosion Inhibitor", CORROSION/99, paper No. 02244, (Houston, TX: NACE, 2002).
15. Y. Sun, K. George and S. Nesic, "The Effect of Cl- and Acetic Acid on Localized $CO_2$ Corrosion in Wet Gas Flow", CORROSION/2003, paper No. 03327 (Houston, TX: NACE, 2003).
16. G. Schmitt and S. Feinen, "Effect of Anions and Cations on the Pit Initiation in $CO_2$ Corrosion of Iron and Steel", CORROSION/2000, paper No. 00001, (Houston, TX: NACE, 2000).
17. Y. Sun, "Localized $CO_2$ Corrosion in Horizontal Wet Gas Flow", Dissertation of Ohio University, 2003.
18. V. Ruzic, "Mechanisms of protective $FeCO_3$ scale removal in single-phase flow-accelerated $CO_2$ corrosion of mild steel", PhD thesis, The University of Queensland, 2005
19. J. Marsh, J. W. Palmer and R. C. Newman, "Evaluation of Inhibitor Performance for Protection against Localized Corrosion", NACE CORROSION/2002, paper No. 288.
20. A. Turnbull, D. Coleman, A. J. Griffiths, P. E. Francis and L. Orkney, "Effectiveness of Corrosion Inhibitors in Retarding the Rate of Propagation of Localized Corrosion", Corrosion, Vol. 59, No. 3, 2003, pp. 250-257.
21. Jordy Bruno, P. Wersin and W. Stumm, "On the influence of carbonate in mineral dissolution: II. The solubility of FeCO3 (s) at 25 ºC and 1 atm total pressure", Geochimica et cosmochimica Acta, Vol. 56, 1992, pp. 1149-1155.
22. W. Preis, H. Gamsjäger, "Thermodynamic Investigation of Phase Equilibria in Metal Carbonate–Water–Carbon Dioxide System", Monatshefte für Chemie, 132, 2001, pp. 1327-1346.

23. D. L. Jensen, J. K. Boddum, J. C. Tjell and T. H. Christensen, "The solubility of rhodochrosite ($MnCO_3$) and siderite ($FeCO_3$) in anaerobic aquatic environments", Applied Geochemistry 17, 2002, pp. 503-511.
24. W. Preis and H. Gamsjäger, "Critical evaluation of solubility data: enthalpy of the formation of siderite", Phys. Chem. Chem. Phys., 4, 2002, pp. 4014-4019.
25. C. A. R. Silva, X. Liu and F. J. Millerol, "Solubility of Siderite ($FeCO_3$) in NaCl solutions, Journal of Solution Chemistry, Vol. 31, No. 2, 2002, pp. 97-108.
26. G. M. Marion, D. C. Catling and J. S. Kargel, "Modeling aqueous ferrous iron chemistry at low temperatures with application to Mars", Geochimica et cosmochimica Acta, Vol. 67, No. 22, 2003, pp. 4251-4266.
27. A. Dugstad, "The Importance of $FeCO_3$ Supersaturation on the $CO_2$ Corrosion of Mild steels", CORROSION/92, paper No. 14 (Houston, TX: NACE, 1992).
28. W. Sun, S. Nesic, and R. C. Woollam, "The Effect of Temperature and Ionic Strength on Iron Carbonate ($FeCO_3$) Solubility", Ohio University Advisory Board, Internal repoprt to be published, 2006.
29. M. Nordsveen, S. Nesic, R. Nyborg and A Stangeland, "A Mechanistic Model for Carbon Dioxide Corrosion of Mild Steel in the Presence of Protective Iron Carbonate Scales-Part1: Theory and Verification", Corrosion, Vol. 59, No. 5, 2003, pp. 443-456.
30. S. Nesic, M. Nordsveen, R. Nyborg and A Stangeland, "A Mechanistic Model for $CO_2$ Corrosion with Protective Iron Carbonate Scales", Corrosion/2001, paper No. 01040 (Houston, TX: NACE, 2001).

Table 1. Test matrix for scale removal experiments

| | | |
|---|---|---|
| General conditions | Steel | C1018 |
| | Temperature /°C | 80 |
| | Partial pressure of $CO_2$ /bar | 0.53 |
| | Solution | 1wt% NaCl |
| | Surface area / $cm^2$ | 5.4 |
| Scale formation | Initial pH | 6.3 |
| | Initial iron concentration /ppm | 200 |
| | Rotating speed /rpm | 0 |
| Mechanical scale removal | Initial super saturation (SS) of $FeCO_3$ | 2 |
| | Initial pH | 6.1 |
| | Rotating speed /rpm | 1000, 7000 |
| Chemical scale removal | Initial supersaturation (SS) of $FeCO_3$ | 0.3 |
| | Initial pH | 5.6, 5.8 |
| | Rotating speed /rpm | 100 |
| Chemo-mechanical scale removal | Initial supersaturation (SS) of $FeCO_3$ | 0.3 |
| | Initial pH | 5.8, 5.6 |
| | Rotating speed /rpm | 1000, 7000 |
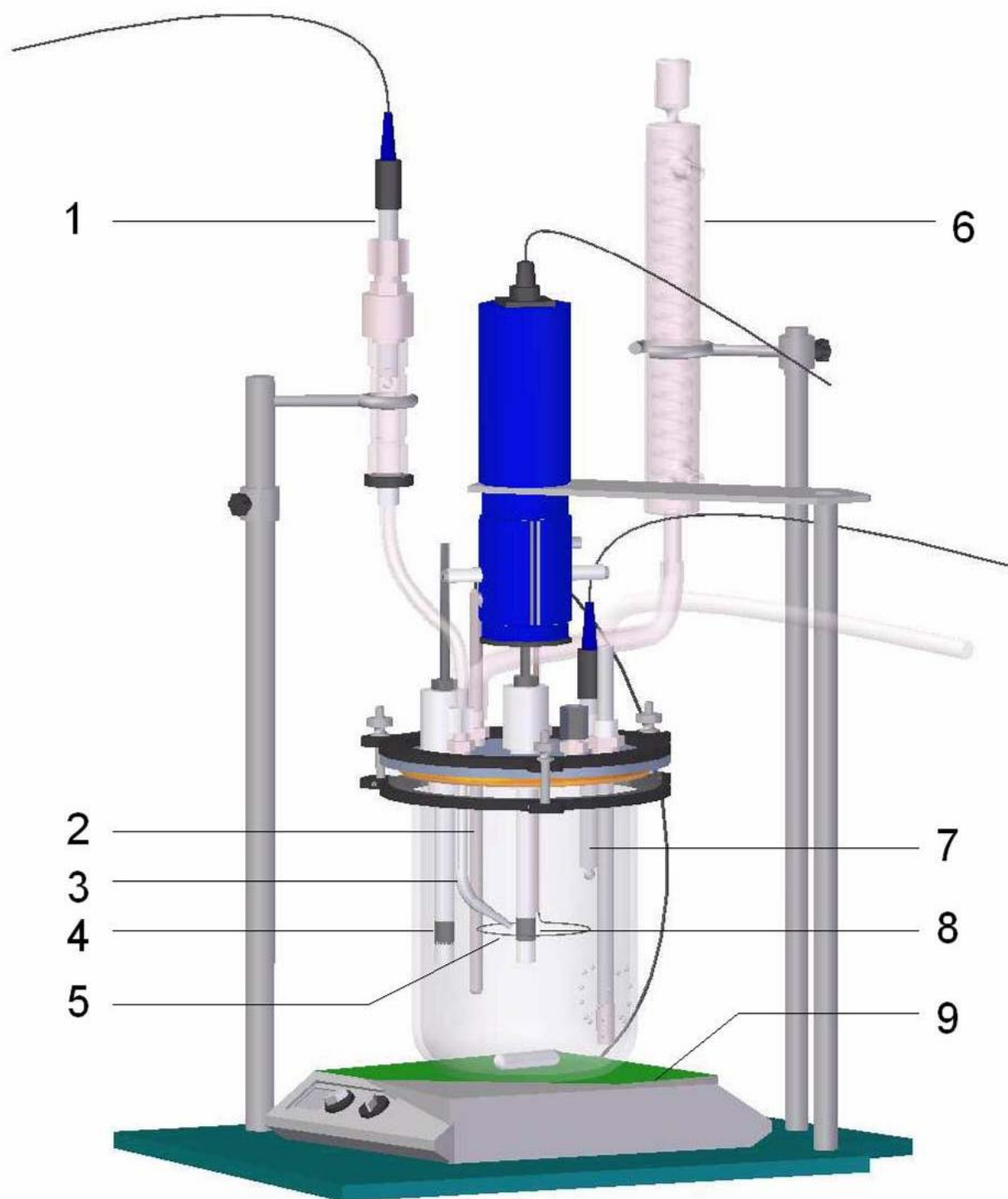
Figure 1. Glass cell set-up for test on localized corrosion initiation. 1- Ag/AgCl reference electrode; 2- thermocouple probe; 3- luggin capillary; 4- additional cylinder electrode, 5- 316 stainless steel wire, 6- condenser, 7- pH probe, 8- rotating cylinder electrode, 9- heat plate
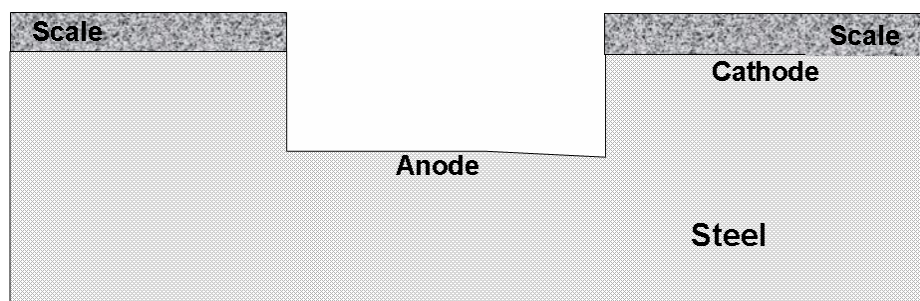
Figure 2.  Configuration of typical localized (mesa) attack in $CO_2$ corrosion for mild steel.
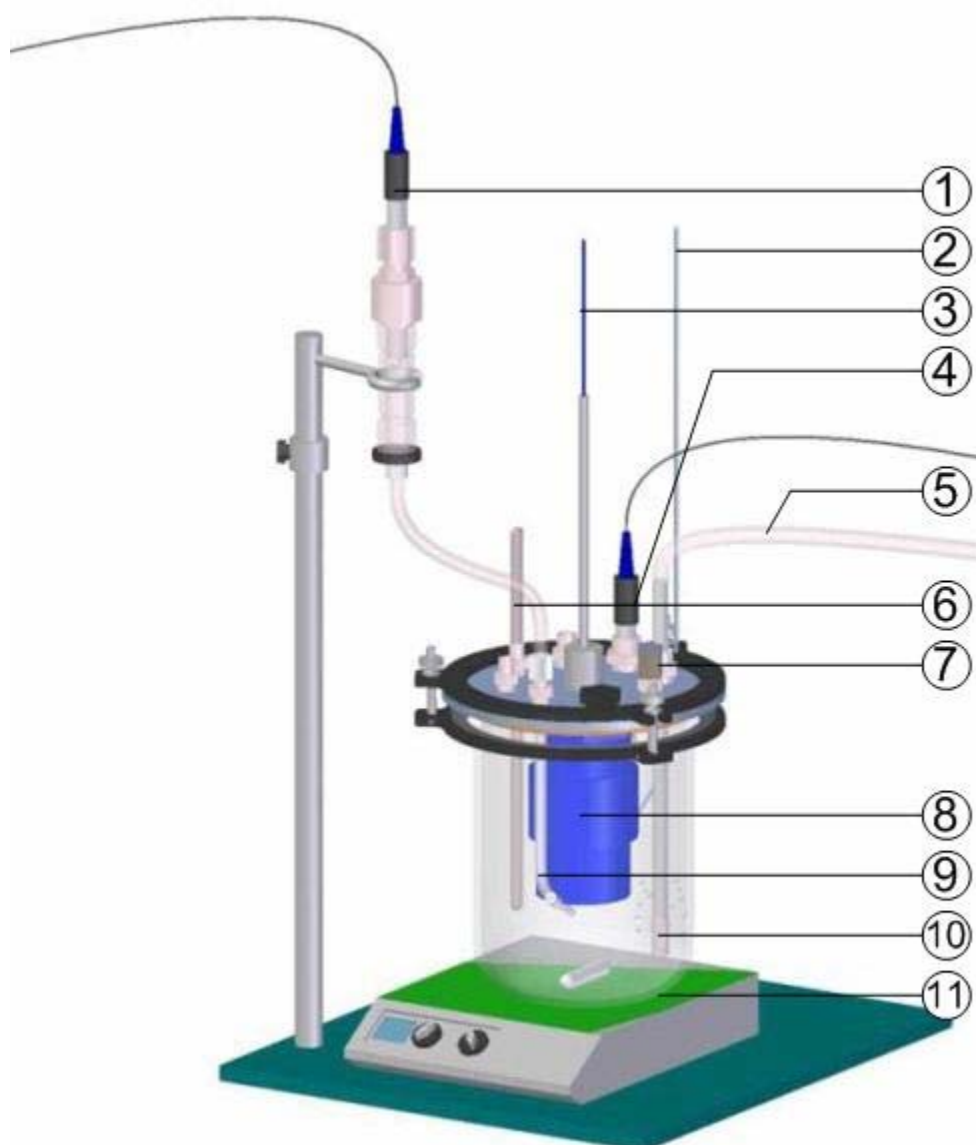


Figure 3.  Glass cell arrangement for the artificial pit test cell. 1- Ag/AgCl reference electrode, 2-wire connection to cathode, 3-wire connection to anode, 4- pH probe , 5-gas inflow, 6- thermocouple probe, 7-gas outflow, 8-artificial pit, 9-luggin capillary, 10-bubbler, 11-heat plate

(a)                                          (b)

(c)                                          (d)
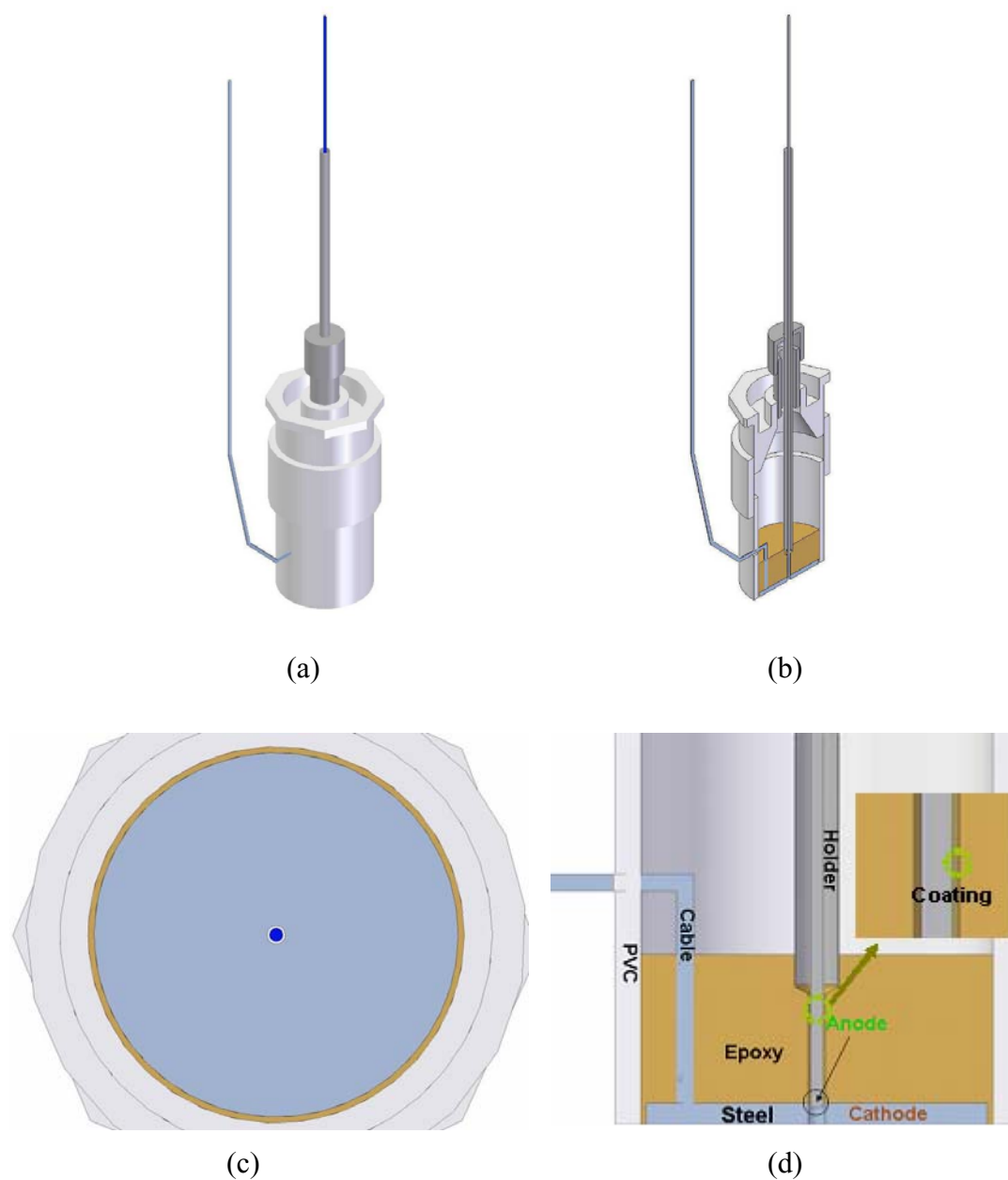
Figure 4  The artificial pit design (a), cutaway (b), enlarged bottom view of cathode (c), and detailed cross section view (d).
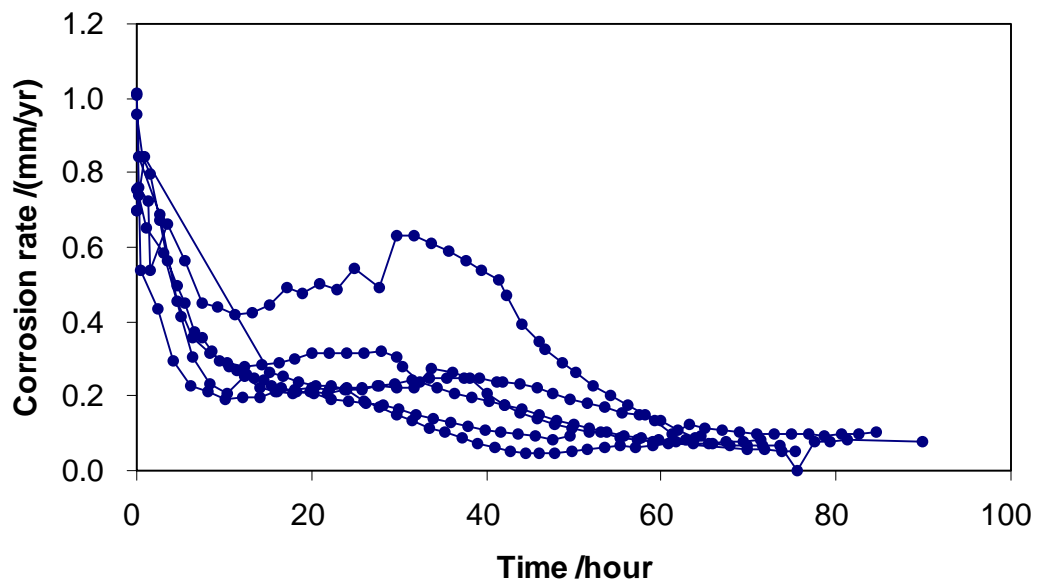
Figure 5. The change of corrosion rate during scale formation process, pH=6.3, initial SS=300, T=80 ºC, pCO₂=0.53bar, [NaCl] =1wt%
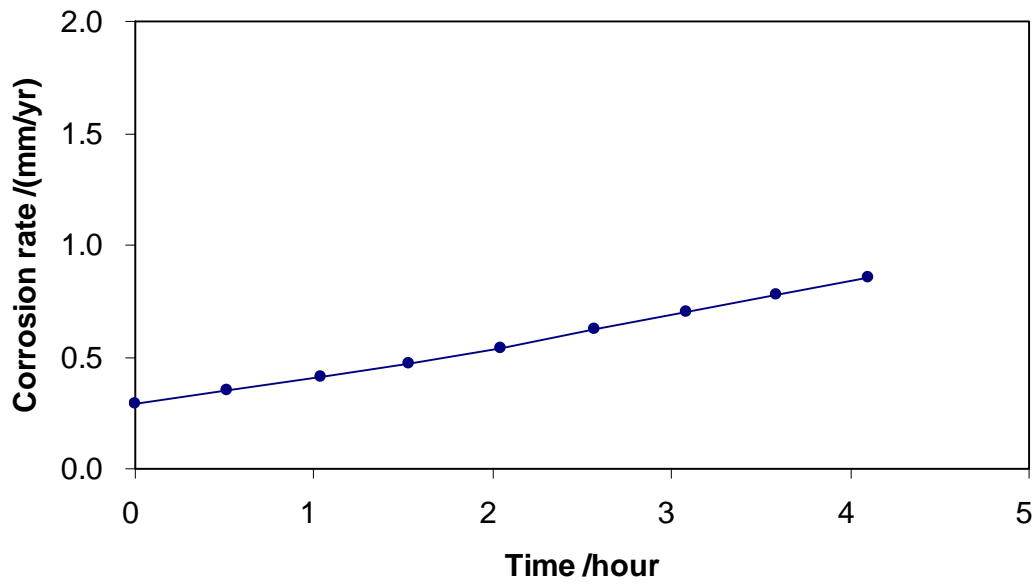
Figure 6. Corrosion rate increase during mechanical scale removal at 1000rpm, pH=6.1, SS=2, T=80 ºC, $pCO_2$=0.53bar, [NaCl] =1wt%
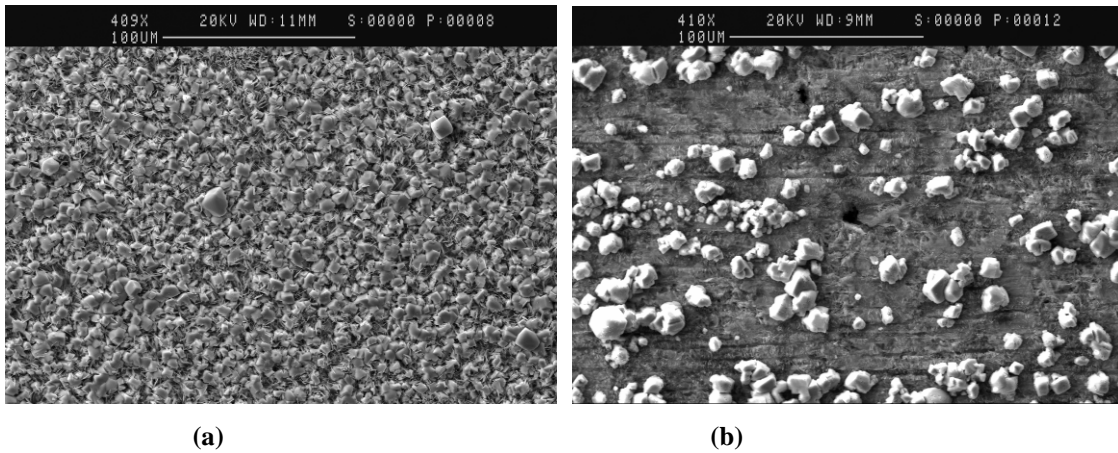


| (a) | (b) |
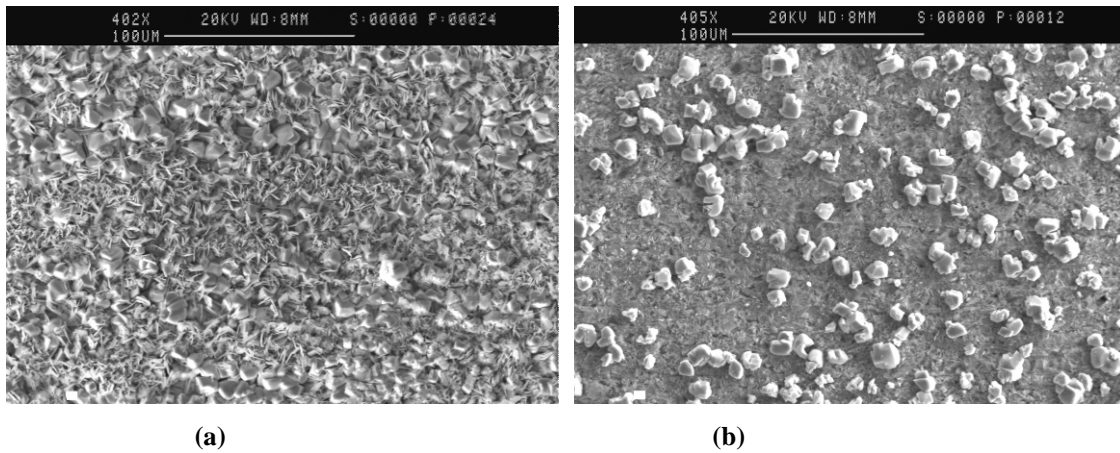
Figure 7. Top view of scale surface before and after mechanical scale removal at 1000rpm. (a) before scale removal and (b) 19 hours after scale removal started. (mag. 400X)
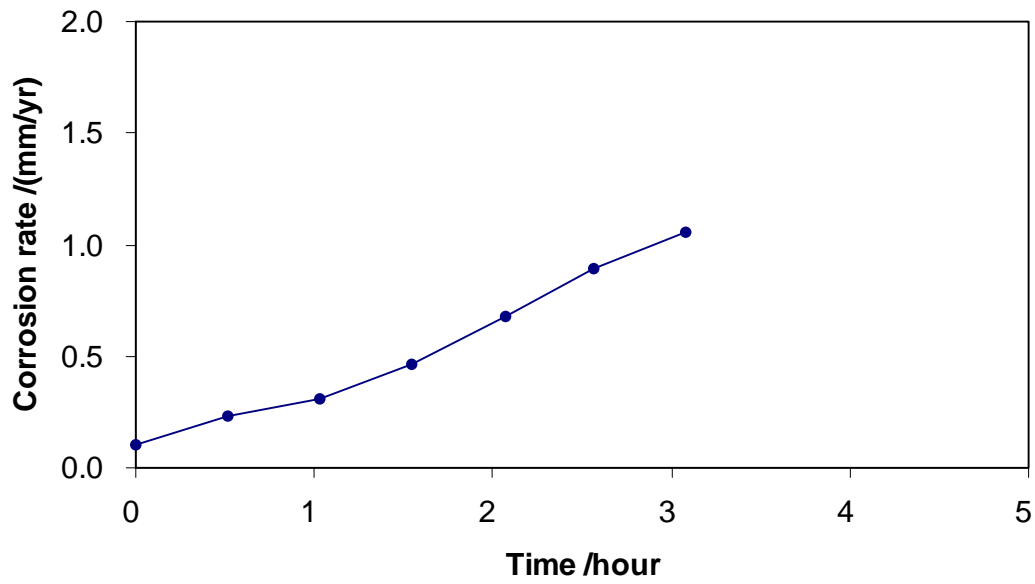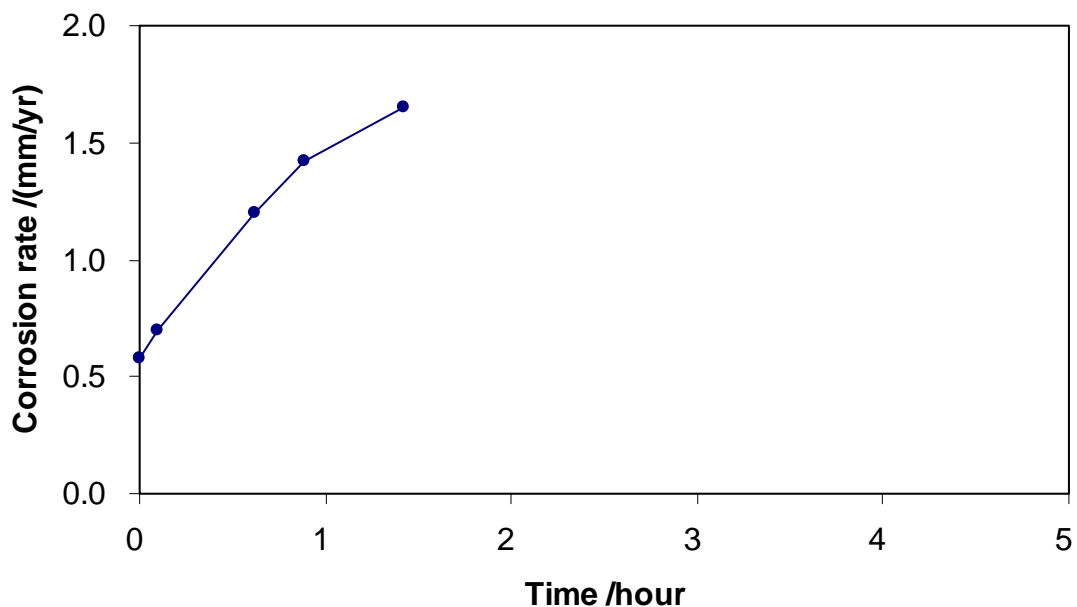
Figure 8. Corrosion rate increase during mechanical scale removal at 7000rpm, pH=6.1, SS=2, T=80 ºC, pCO$_2$=0.53bar, [NaCl] =1wt%
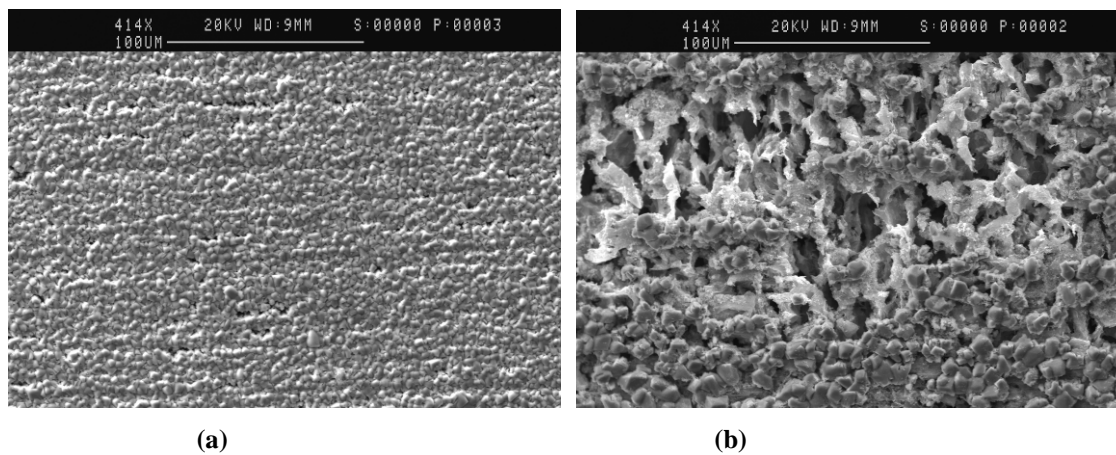


(c)                                                    (d)
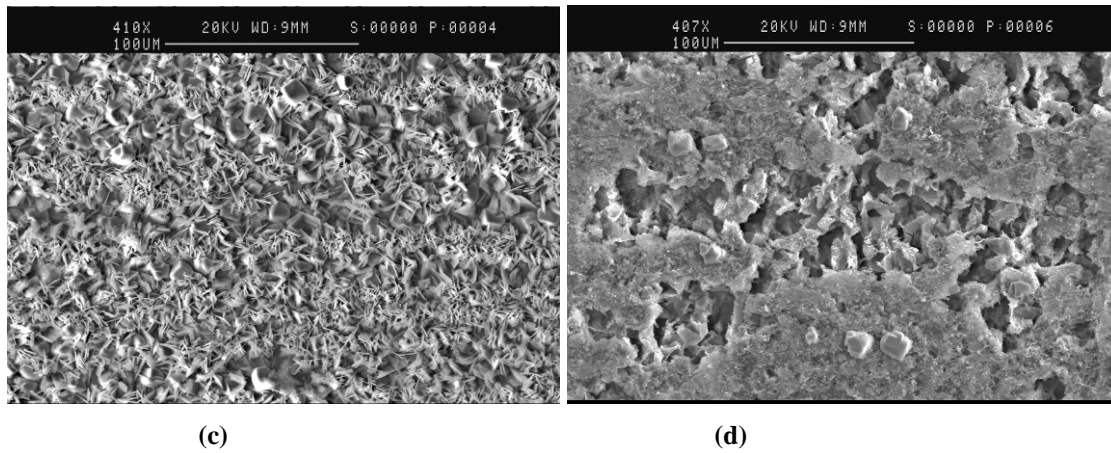
Figure 9. Top view of scale surface before and after mechanical scale removal at 7000rpm. (a) before scale removal and (b) 45 hours after scale removal started. (mag. 400X)
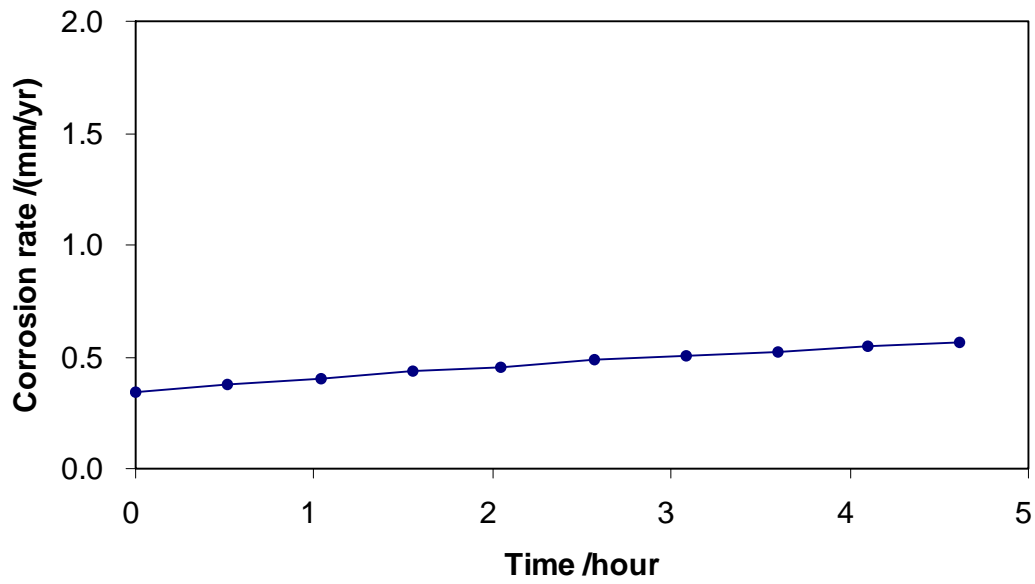
Figure 10. Corrosion rate increase during chemical scale removal at 100rpm, pH=5.8, SS=0.3, T=80 °C, $pCO_2$=0.53bar, [NaCl] =1wt%



**(a)**  **(b)**
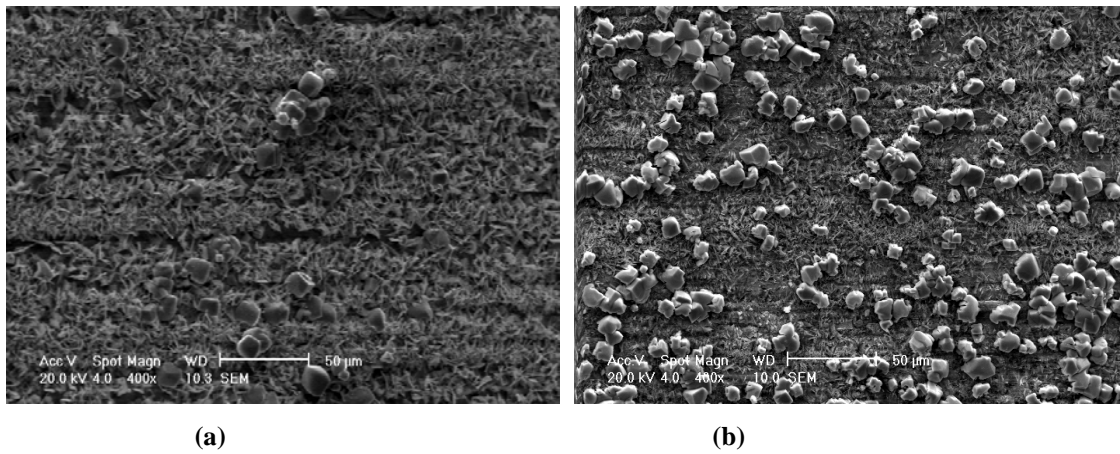
Figure 11. Top view of scale surface before and after chemical scale removal at 100rpm, pH=5.8, SS=0.3. (a) before scale removal and (b) 28 hours after scale removal started. (mag. 400X)
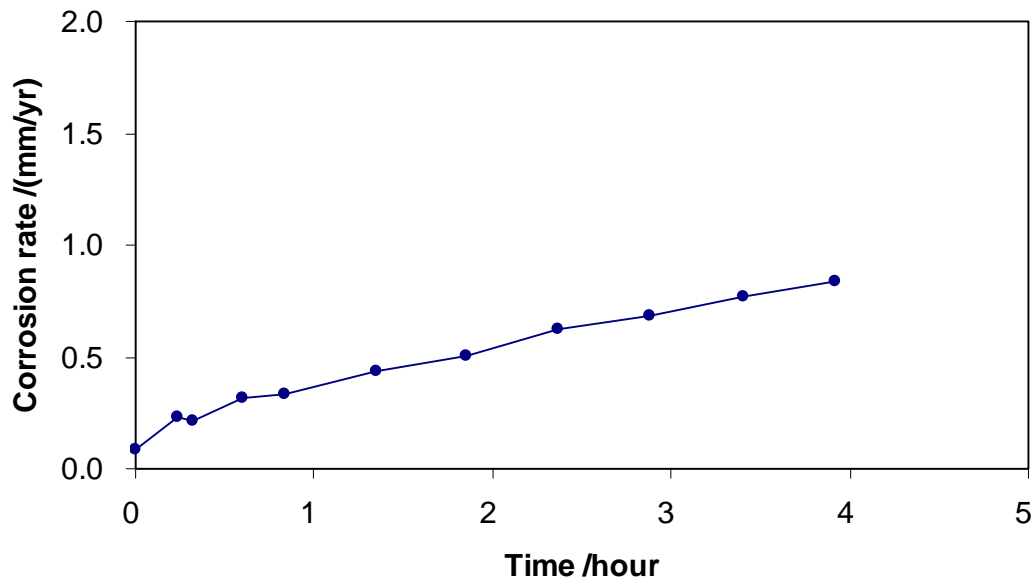
Figure 12. Corrosion rate increase during chemical scale removal at 100rpm, pH=5.6, SS=0.3, T=80 ºC, $pCO_2$=0.53bar, [NaCl] =1wt%



(a)                                                                                           (b)
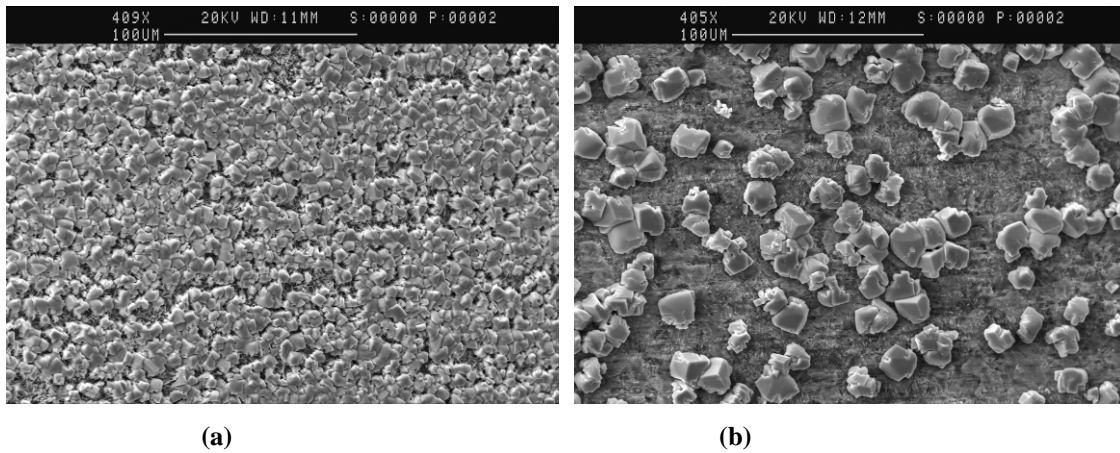
Figure 13. Top view of scale surface before and after chemical scale removal at 100rpm, pH=5.6, SS=0.3. (a) before scale removal and (b) 45 hours after scale removal started. (mag. 400X)
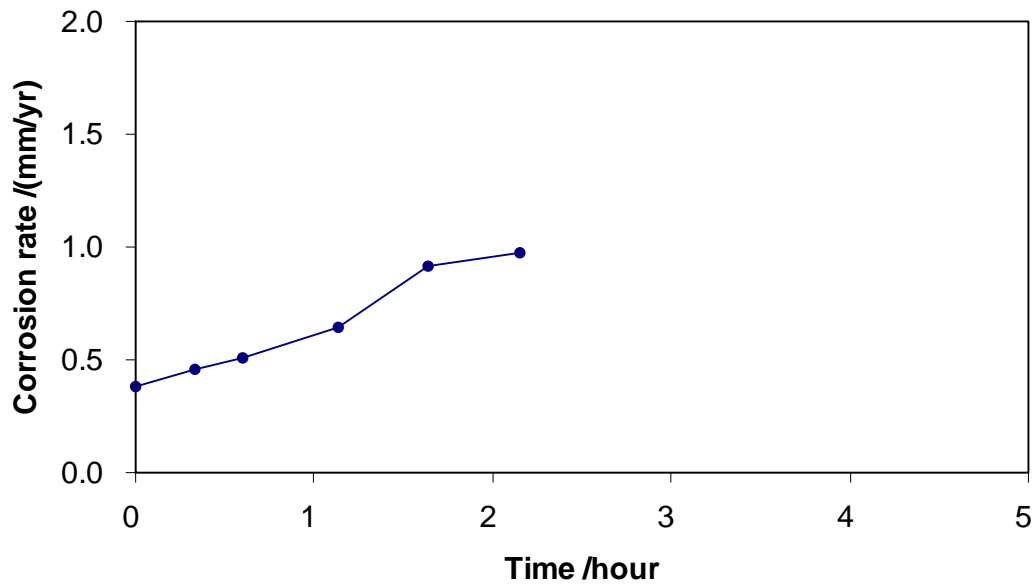
Figure 14. Corrosion rate increase during combined chemo-mechanical scale removal process, pH=5.8, rotating speed=1000rpm, SS=0.3, T=80 ºC, $pCO_2$=0.53bar, [NaCl] =1wt%



(a)                                                                 (b)

Figure 15. Top view of scale surface before and after chemo-mechanicall scale removal at 1000rpm, pH=5.8, SS=0.3. (a) before scale removal and (b) 46 hours after scale removal started. (mag. 400X)

Figure 16. Corrosion rate increase during combined chemo-mechanical scale removal process, pH=5.6, rotating speed=7000rpm, SS=0.3, T=80 ºC, $pCO_2$=0.53bar, [NaCl] =1wt%



| (a) | (b) |

Figure 17. Top view of scale surface before and after chemo-mechanical scale removal at 7000rpm, pH=5.6, SS=0.3. (a) before scale removal and (b) 56 hours after scale removal started. (mag. 400X)
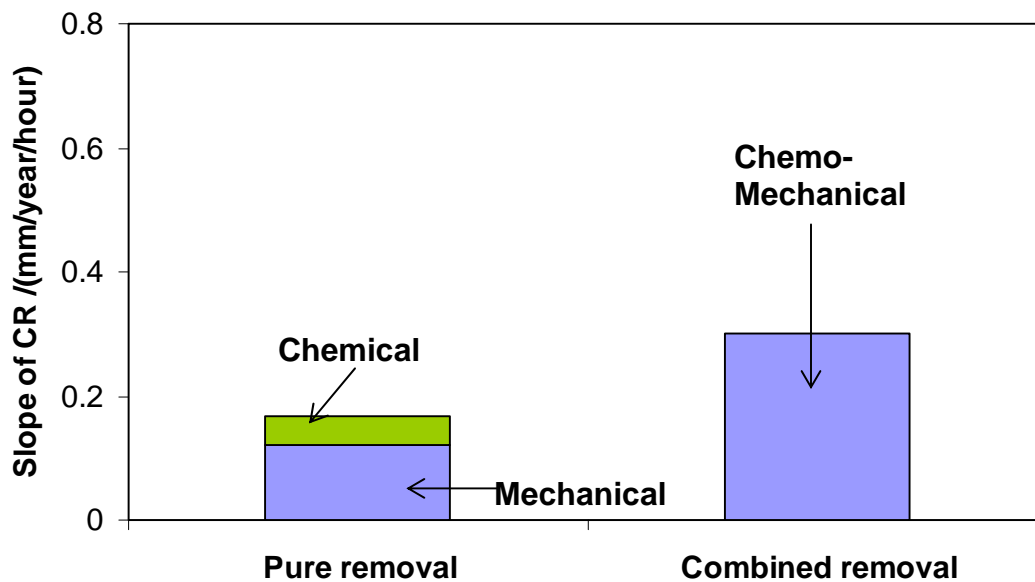
Figure 18. Comparison of slopes of corrosion rate curves of mechanical (1000rpm), chemical (pH5.8) and chemo-mechanical (pH5.8, 1000rpm) scale removal
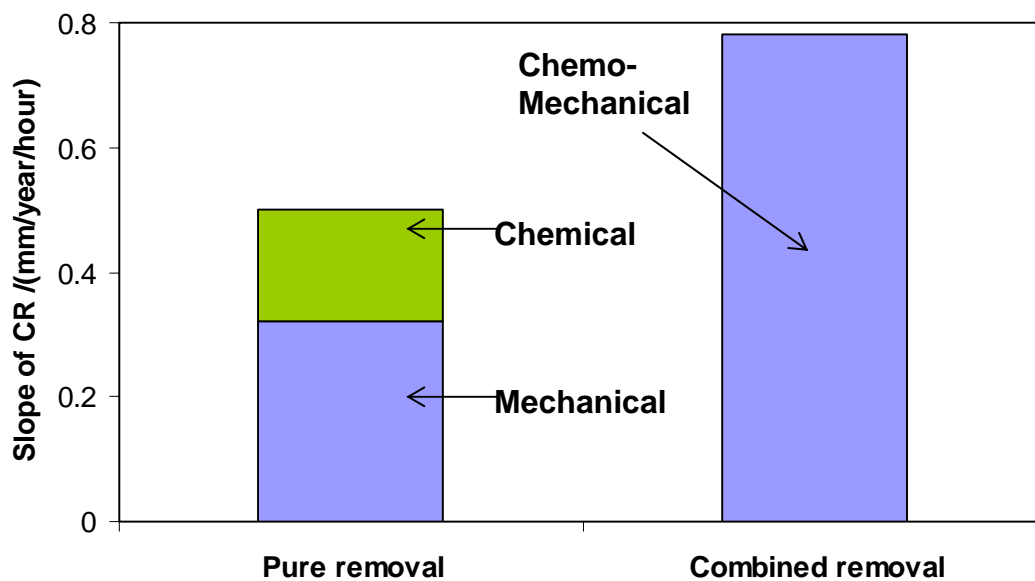


Figure 19. Comparison of slopes of corrosion rate curves of mechanical (7000rpm), chemical (pH5.6) and chemo-mechanical (pH5.6, 7000rpm) scale removal
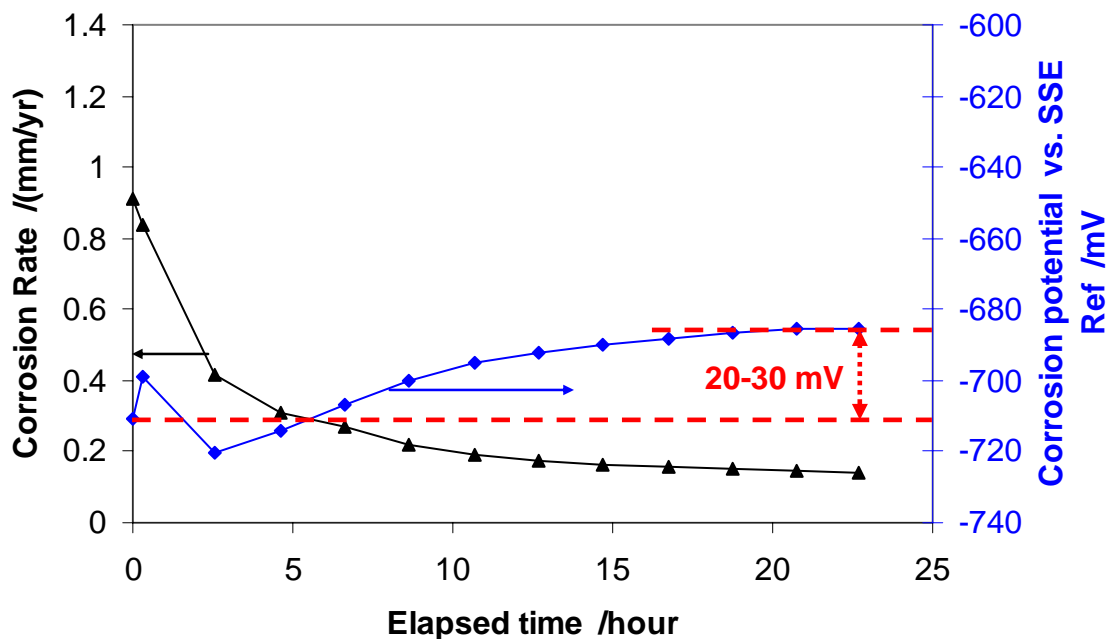
Figure 20  Corrosion rate and open circuit potential vs. saturated Ag/AgCl reference electrode (SSE) history for a typical iron carbonate scale formation process during AP test. SEM images illustrate the appearance of the steel surface at the beginning and the end of the scale forming process
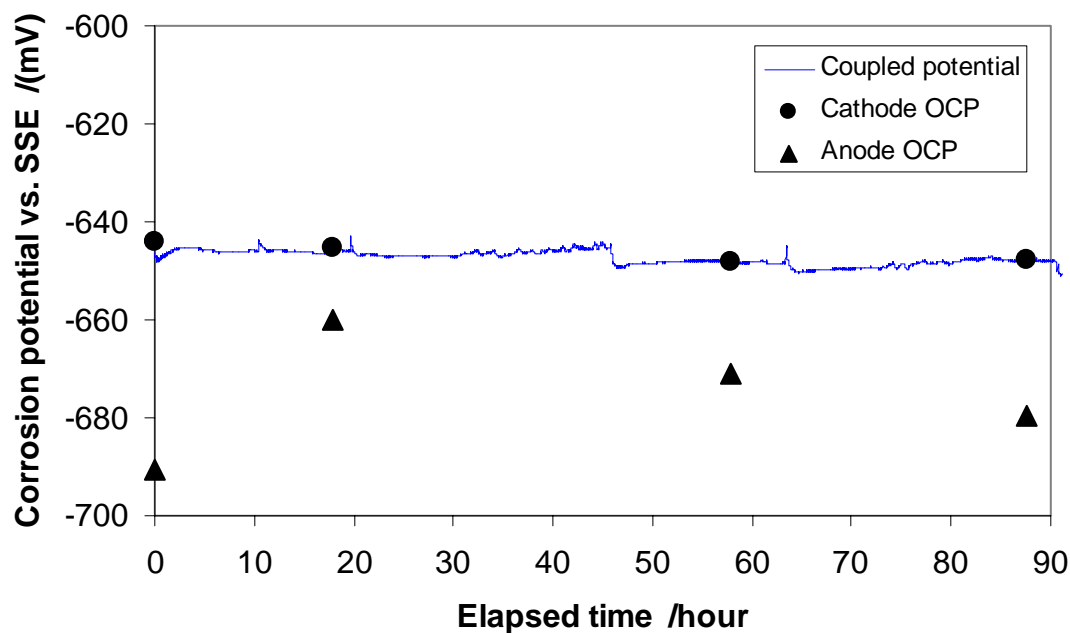


Figure 21  Open circuit potentials (OCP) of anode and cathode and coupled (shorted) potential (vs. SSE) between them at pH=5.9, T=80°C, SS=1-4, pit depth=0 mm, 1wt % NaCl, stagnant
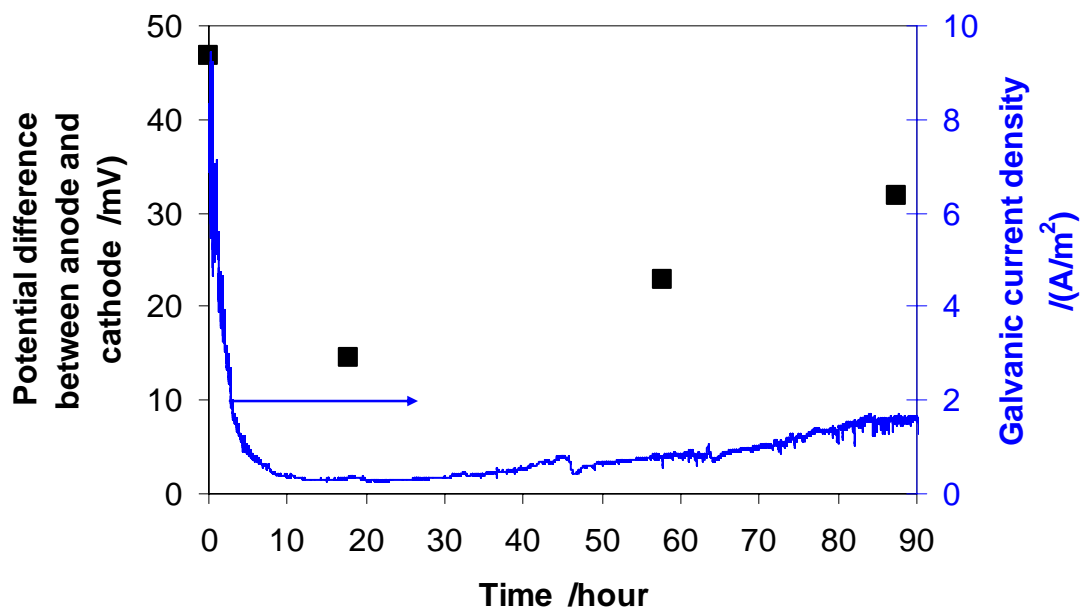
Figure 22  The open circuit potential difference between anode and cathode and galvanic current at pH=5.9, T=80°C, SS=1-4, pit depth=0 mm, 1wt % NaCl, stagnant
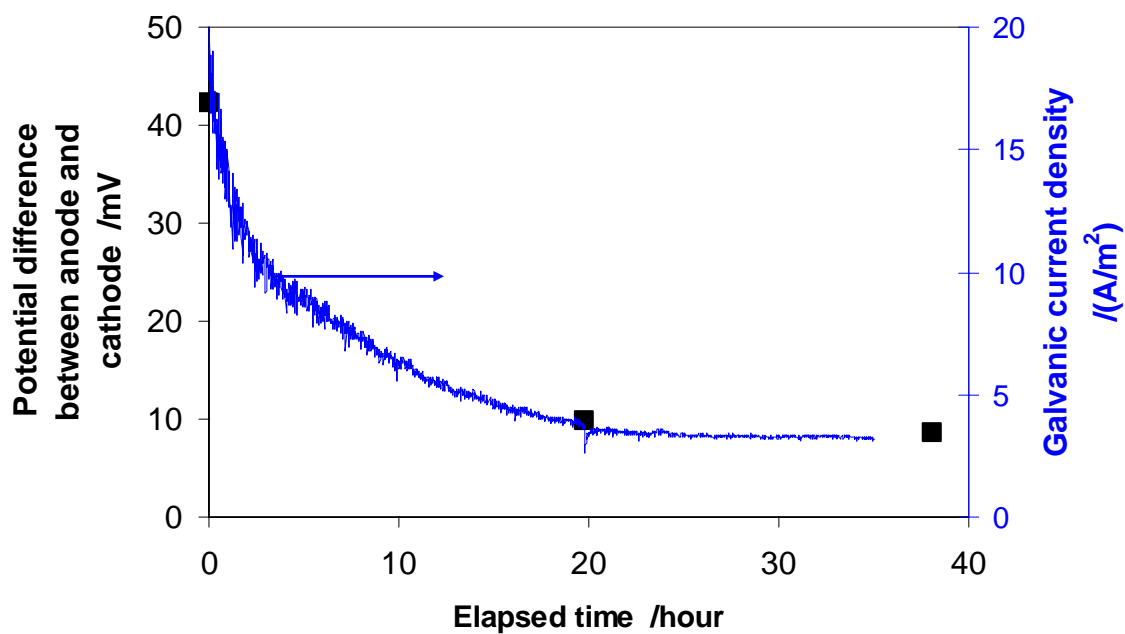


Figure 23  The open circuit potential difference between anode and cathode and galvanic current at pH=5.9, T=80°C, SS=1-4, pit depth=0 mm, 1wt % NaCl, rotation=500 rpm
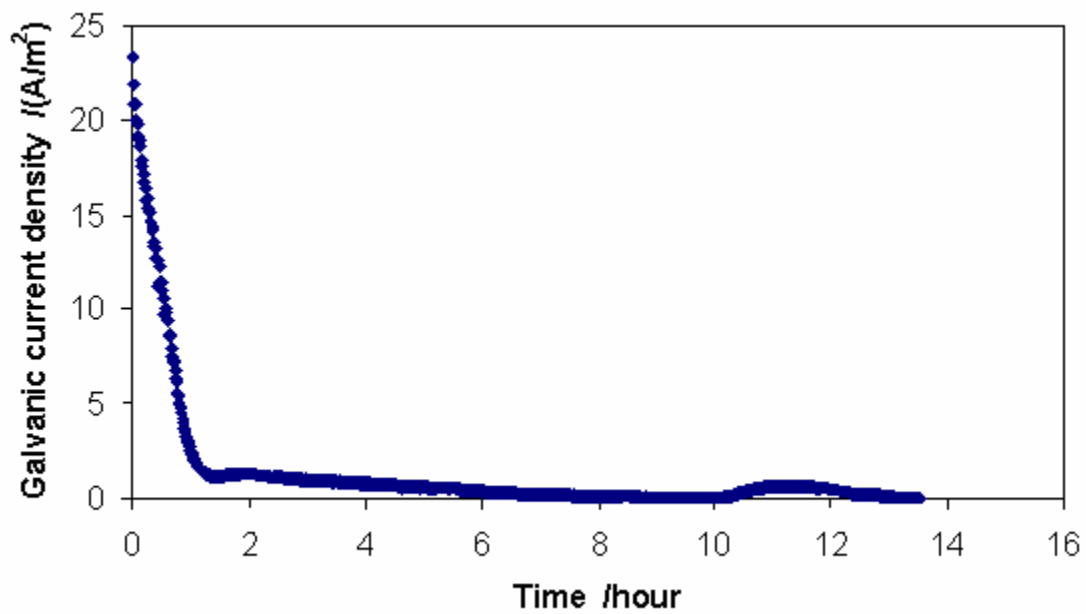
Figure 24 Artificial pit becomes passive at high $FeCO_3$ supersaturation (SS= 3-9) under T=80 ºC, $pCO_2$=0.53bar, pH=5.5, [NaCl] =1wt%.
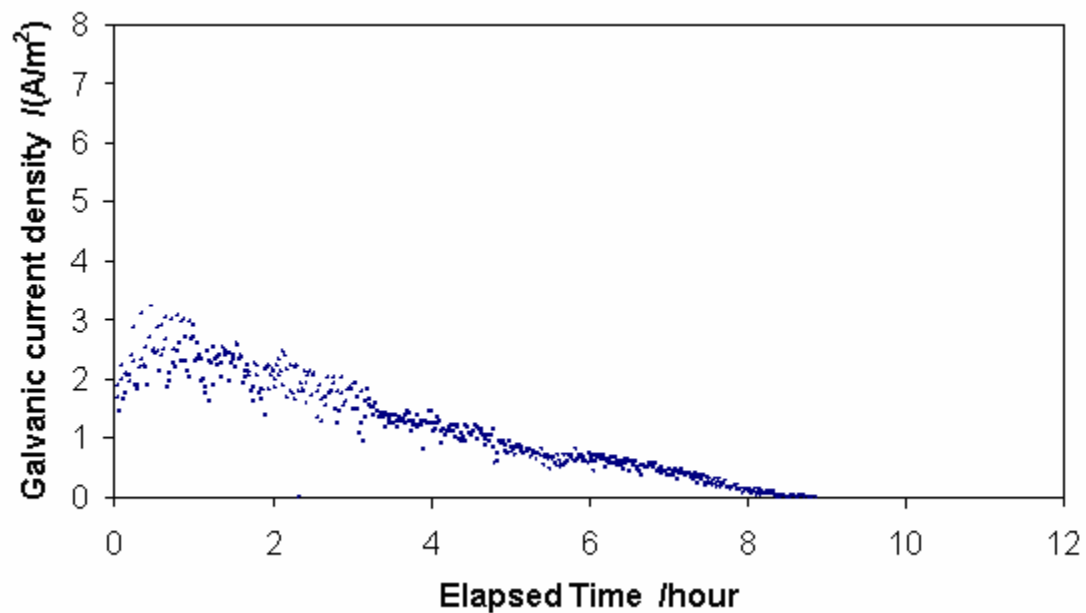


Figure 25  Artificial pit becomes passive at low $FeCO_3$ supersaturation (SS=0.2-0.5) under T=80 ºC, $pCO_2$=0.53bar, pH=5.8, [NaCl] =1wt%.
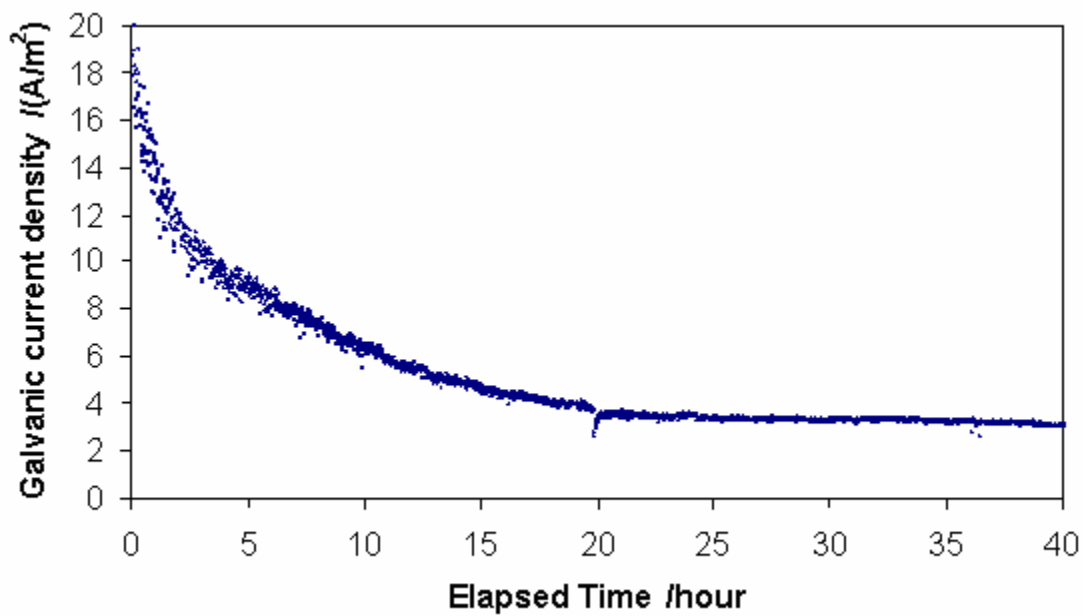
Figure 26  Artificial pit is active at moderate $FeCO_3$ supersaturation under  (SS=0.4-4) T=80 ºC, $pCO_2$=0.53bar, pH=5.9, [NaCl] =1wt%.
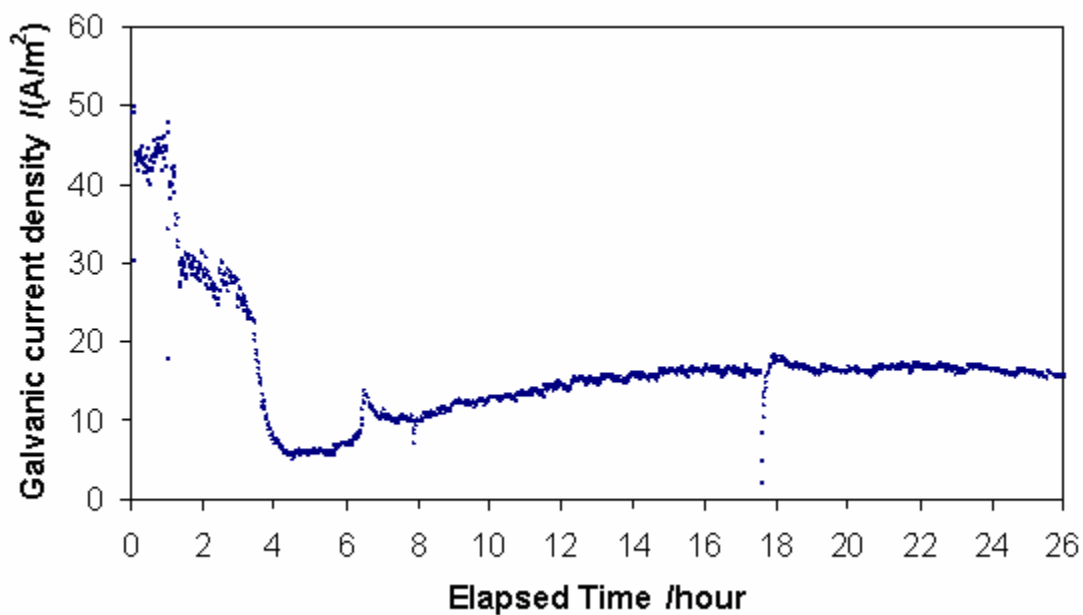


Figure 27  Artificial pit is active at moderate $FeCO_3$ supersaturation (SS=0.3-0.8) under T=80 ºC, $pCO_2$=0.53bar, pH=6.0, [NaCl] =10wt%.